GLONASS-K2 signal analysis

S. Thoelert[1] · **P. Steigenberger[2]** · **O. Montenbruck[2]**

Abstract

K2 is a new generation of GLONASS satellites that provides code division multiple access (CDMA) signals in the L1, L2 and L3 frequency bands in addition to legacy L1 and L2 signals based on frequency division multiple access (FDMA) modulation. The first GLONASS-K2 satellite was launched in August 2023 and started signal transmission in early September 2023. Based on measurements with a 30-m high-gain antenna, spectral characteristics of the various signal components are described and relative power levels are identified. A 3 dB (L1) to 4 dB (L2) higher total power is determined for the CDMA signal compared to the legacy FDMA signal and an equal power of the open service and secured CDMA signal components is found. The ranging code of the L2 channel for service information, which has not been publicly disclosed so far, is identified as a Gold code sequence consistent with the data channel of the L1 open service CDMA signal. The high-gain antenna measurements are complemented by tracking data from terrestrial receivers that enable a first assessment of user performance. An up to 50% improvement in terms of noise and multipath performance is demonstrated for the new L1 and L2 CDMA signals in comparison with their legacy counterpart, but no obvious differences between the different binary phase-shift keying and binary offset carrier modulations of the data and pilot components of these signals could be identified for the test stations. Triple-frequency carrier phase observations from L1, L2, and L3 CDMA signals exhibit good consistency at the noise and multipath level, except for small variations that can be attributed to slightly different antenna phase patterns on the individual frequencies. Overall, the new CDMA signals are expected to notably improve and facilitate precise point positioning applications once fully deployed across the GLONASS constellation.

Keywords GLONASS · CDMA · FDMA · Spectrum · Signal analysis

Introduction

The Russian Global'naya Navigatsionnaya Sputnikovaya Sistema (GLONASS; Revnivykh et al. 2017; Langley 1997), has traditionally used frequency division multiple access (FDMA) signals in the L1 and L2 frequency band (RISDE 2008). Here, all satellites use a common modulation and ranging code, but transmit their signals at slightly different frequencies separated by multiples of about 0.5 MHz. More specifically, the signal frequencies are specified as

$$f_{L1,k} = 1602.0\,\text{MHz} + k \cdot 0.5625\,\text{MHz}$$
$$f_{L2,k} = 1246.0\,\text{MHz} + k \cdot 0.4375\,\text{MHz} \tag{1}$$

with frequency channel numbers k ranging from -7 to $+6$ (RISDE 2008). In view of a limited number of available frequency bands, anti-podal satellites, i.e., satellites at opposite locations in the same orbital plane, are typically assigned the same frequency.

The FDMA signals in both bands provide an open service (L1OF, L2OF; PNT IAC 2020) as well as a secured service (L1SF, L2SF). In analogy with GPS, the corresponding signals are commonly labeled as C/A- and P-code and modulated in quadrature phase-shift keying (QPSK) modulation. The ranging code of the secured service signals has not been publicly released by the GLONASS authorities, but is apparently unencrypted. Early analyses by Lennen (1989) suggest the use of a 25-bit maximum length shift register code truncated to a 1-s duration, based on which most geodetic GNSS

✉ S. Thoelert
  steffen.thoelert@dlr.de

1 Deutsches Zentrum für Luft- und Raumfahrt, Institute
   of Communications and Navigation, 82234 Weßling,
   Germany

2 Deutsches Zentrum für Luft- und Raumfahrt, German Space
   Operations Center, 82234 Weßling, Germany

receivers are able today to track the GLONASS P-code in addition to the open C/A-code on both frequencies.

Starting with the first GLONASS-K1 satellite, R801, an L3 code division multiple access (CDMA) open service signal (L3OC) at 1202.025 MHz was introduced in 2011 (RSS 2016c). The R801 satellite transmits the L3 CDMA signal via a dedicated antenna, whereas all other K1 satellites use the same antenna for L1/L2 FDMA and L3 CDMA signals. In order to distinguish these different satellite types, they are labeled as GLONASS-K1A and -K1B, respectively, within the International GNSS Service (IGS, Johnston et al. 2017). GLONASS-M+ spacecraft, launched since 2014, also transmit the L3 CDMA signal from a dedicated antenna like K1A. Early analyses have evidenced a good signal quality and a high power level of the L3OC signal (Thoelert et al. 2011) and demonstrated the benefit of CDMA signals for precise positioning with ambiguity resolution (Zaminpardaz et al. 2017).

K2 is the latest generation of GLONASS satellites and adds the ability to transmit L1 and L2 CDMA signals at 1600.995 and 1248.06 MHz (RSS 2016a, b). The FDMA and CDMA signals on the first K2 satellite, R803, launched in August 2023, are transmitted from two separate antenna arrays shown in Fig. 1 using synchronized carriers. Similar to GPS and other GLONASS satellites, both arrays are composed of 12 helix antennas arranged in an inner ring of four elements and an outer ring of eight elements to obtain an M-type gain pattern with a uniform flux over the entire surface of the Earth (Maqsood et al. 2017). Constant envelope multiplexing concepts enabling joint transmission of FDMA and CDMA signals through a common amplifier and antenna are presented in Biryukov (2018) and Bakitko (2021), but not required on R803 and mainly considered for future versions of GLONASS-K satellites with a single navigation antenna. An early spectrum of R803 presented in Karutin (2023) shows the characteristic main and side lobes
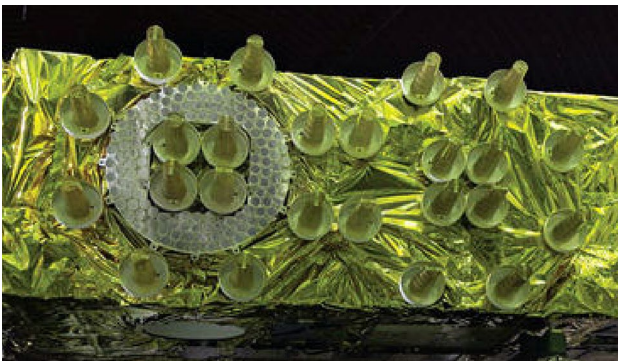

Fig. 1 Image of the CDMA (left, with integrated laser retroreflector array) and FDMA (right) transmit antenna arrays of GLONASS-K2. Image courtesy of ISS Reshetnev

of legacy (L1OF, L1SF) and modernized (L1OC, L1SC) signals in the L1 band.

The present study provides a comprehensive analysis of the new L1 and L2 CDMA signals transmitted by the first GLONASS-K2 satellite. In the following section the spectral characteristics of the open and secured signals are investigated based on measurements with a high-gain dish-antenna. Relative power levels and specific modulation properties are identified from the composite spectrum and IQ-constellation diagrams. The analysis of high-gain antenna data is complemented by the assessment of early receiver data illustrating the signal quality and measurement performance from a user's point of view. Aside from noise and multipath characteristics, the coherence of the L1, L2, and L3 CDMA carriers is evaluated.

GLONASS-K2 signals

An overview of the various signals transmitted by the first GLONASS-K2 satellite is given in Table 1. The individual signals make use of different modulation schemes including binary and quadrature phase-shift keying (BPSK/QPSK) as well as binary offset carrier (BOC) modulation to achieve a spectral separation of individual components. Chipping rates of the respective ranging codes vary between 0.5115 and 10.23 MHz.

In total, 12 different signals and channels in the L1, L2, and L3 frequency bands are provided, including seven open and four secured components. The L2 CDMA signal, furthermore, includes a "channel for service information" (CSI). It currently lacks a public specification, and it remains unclear, whether the CSI provides an open, secured, or commercial service.

In the following, measurements of a 30-m high-gain antenna are used for a detailed analysis of the GLONASS-K2 signals. The antenna is located at the Weilheim ground station of the German Space Operations Center (GSOC) and is regularly used for GNSS signal analysis (e.g., Montenbruck et al. 2006; Thoelert et al. 2012, 2019a, b). The antenna provides a gain of about 50 dB, which results in peak spectral flux densities (SFDs) of common GNSS signals that exceed the noise floor by range 30-40 dB. Further details on the measurement facility are given in Thoelert et al. (2009). For the present study, raw in-phase and quadrature samples of the received signal in the L1, L2 and L3 band were collected with a spectrum signal analyzer after mixing with reference frequencies of 1602 MHz, 1246 MHz, and 1202 MHz, respectively. The selected sampling frequency of 122.8 MHz and a 96 MHz bandwidth offer adequate resolution for the spectrum analysis and the characterization of chip transitions.

Table 1 Signals transmitted by GLONASS R803

Band	Signal	Frequency (MHz)	Modulation	Chip rate (MHz)	Comment	Reference(s)
L1 FDMA	L1OF (C/A)	1598.625	BPSK(0.5)	0.511	Open service	RISDE (2008)
	L1SF (P)		BPSK(5)	5.11	Secured service, unencrypted	Karutin (2012)
L2 FDMA	L2OF (C/A)	1243.375	BPSK(0.5)	0.511	Open service	RISDE (2008)
	L1SF (P)		BPSK(5)	5.11	Secured service, unencrypted	Karutin (2012)
L1 CDMA	L1OCd	1600.995	BPSK(1)	0.5115	Open service, data signal	Karutin (2012); RSS (2016a)
	L1OCp		BOC(1,1)	0.5115	Open service, pilot signal	Karutin (2012); RSS (2016a)
	L1SC		BOC(5,2.5)	2.5575	Secured service	Karutin (2012)
L2 CDMA	L2 CSI	1248.06	BPSK(1)	0.5115	Channel for service information	Karutin (2012)
	L2OCp		BOC(1,1)	0.5115	Open service, pilot signal	Karutin (2012); RSS (2016b)
	L2SC		BOC(5,2.5)	2.5575	Secured service	Karutin (2012)
L3 CDMA	L3OCd	1202.025	BPSK(10)	10.23	Open service, data signal	RSS (2016c)
	L3ODp		BPSK(10)	10.23	Open service, pilot signal	RSS (2016c)

The FDMA frequencies refer to frequency channel number $k = -6$

L1 signal components

A spectrum of the upper L-band showing the SFD of the compound L1 FDMA and CDMA signals of R803 is shown in Fig. 2. Most of the energy is transmitted in a range of about 1593–1609 MHz, but the spectrum in this region is notably asymmetric due to the 2.3 MHz shift of the FDMA and CDMA center frequencies. It should be noted, though, that this asymmetry depends largely on the FDMA frequency channel (here, $k = -6$) and a slightly different spectrum arises, when another channel is assigned. Aside from a narrow peak 1598.625 MHz reflecting the 0.5 MHz C/A-code of the L1OF signal, three adjacent lobes of about 5 MHz width and separation can be recognized. While the outer lobes result from the BOC(5,2.5) modulation of the secured L1OS signal, the central lobe at 1600.995 MHz relates to the open L1 CDMA signal and is actually made up of two distinct components. More specifically, it results from the time-multiplexing of the BPSK(1)-like data channel with a width of 1 MHz and the BOC(1,1)-like pilot signal with two distinct main lobes at ± 1 MHz relative to the center frequency.

In accord with the open service signal specification (RSS 2016a), which indicates aligned edges of the subcarrier meander code and the ranging code sequence, the spectrum of the BOC(1,1) component best matches a $BOC(1,1)_{sin}$ modulation. Use of a BOC_{sin}-type modulation is likewise suggested for the secured signal L1SC by the observed CDMA spectrum.

The composition of the overall spectrum is illustrated by the modeled spectra of it's individual constituents in panels (b) and (c) of Fig. 2. These, as well as the resulting sum in panel (a) are based on the simplifying assumption of infinite bandwidth and partly exceed the power of the real signals at large offsets from the center frequency. However, only a moderate (< 5 dB) attenuation can be observed over a range of ± 40 MHz around the center frequencies, suggesting that the signal generation and transmission chain of the new K2 satellite does not include a sharp bandpass filter. On the other hand, the L1 signals are intentionally suppressed by a notch filter for frequencies of 1610.6–1613.8 MHz. This reflects a general GLONASS policy (RISDE 2008; Langley 1997) and aims to avoid transmission of GNSS signals in a protected radio astronomy band in accord with regulations of the International Telecommunications Union (ITU).

Based on the measured spectral flux density, the received power levels of the L1OF, L1SF, L1OCd, and L1OCp signals agree among each other to better than 1 dB and correspond to an effective isotropic radiated power (EIRP) of 29.5 dBW per signal. A roughly 3 dB higher power applies for the L1SC signal, implying a similar strength of the open (data+pilot) and the secured CDMA signal. Since FDMA and CDMA signals are transmitted by different antennas (and amplifiers), only two or three signals need to be combined in each chain. In both cases, a constant power envelope is readily achieved by modulating the open and secured signals in phase quadrature. This technique is combined with time multiplexing of the data and pilot channels, implying a 1:1 power sharing for these signal components.

An IQ constellation diagram of the combined L1 CDMA and FDMA signals is shown in Fig. 3. It provides a heat map representing the probability density of in-phase (I)

Fig. 2 GLONASS-K2 (R803) spectral flux density (SFD) in the L1 frequency band as collected with the Weilheim 30-m dish-antenna on January 17, 2024 (**a**). For illustration, modeled infinite-bandwidth spectra of the individual FDMA signals (centered at 1598.625 MHz) and CDMA signals (centered at 1600.995 MHz) signals are shown in panels (**b**) and (**c**), respectively. The sum of all these individual signals gives the *modeled* curve shown in red in panel (**a**)
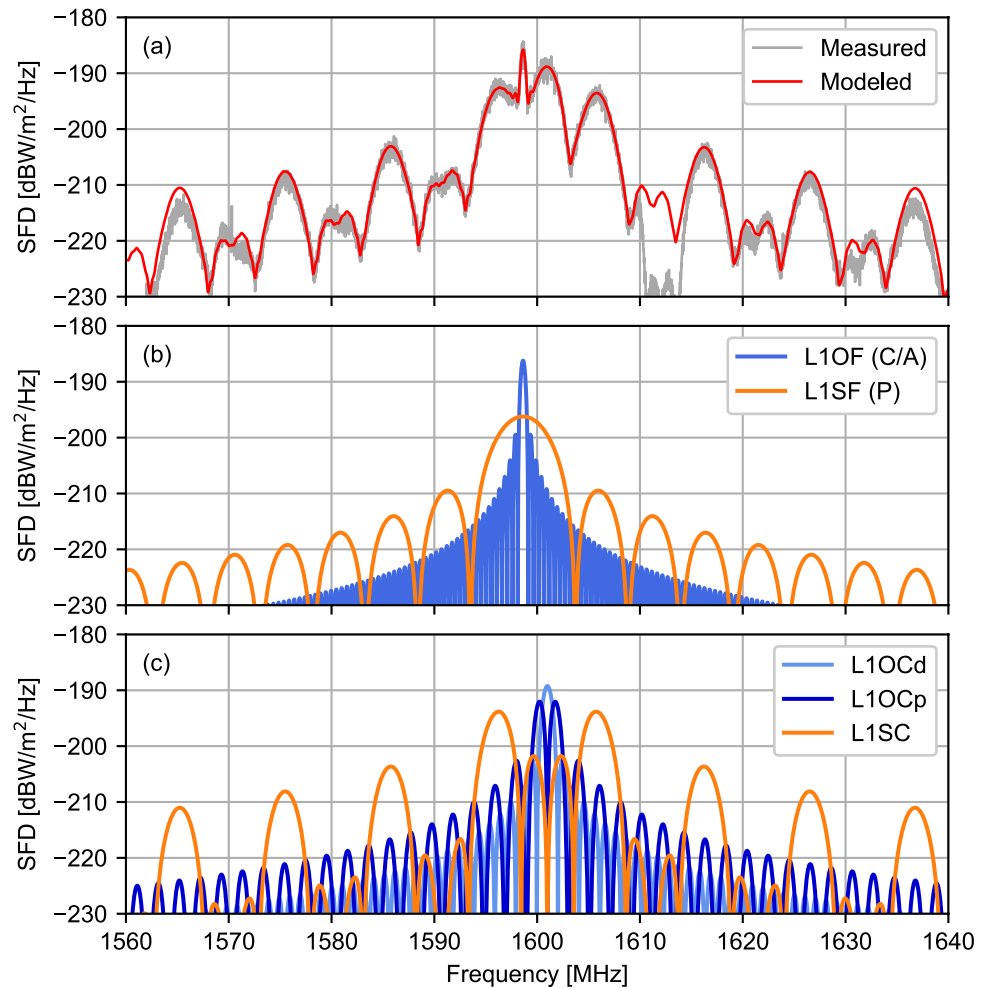
and quadrature (Q) signal components after mixing of the received signal with the Doppler-compensated L1 CDMA frequency and normalization to the approximate CDMA amplitude. Red dots indicate the approximate location of IQ values for chip transitions of the L1SC and L1OC CDMA components. They largely match a square that would be expected for an ideal QPSK modulation with L1OC and L1SC components of equal amplitude. The actual signal shows a deviation from orthogonality of about 3° and amplitude differences of the I and Q component at the level of about 5%. However, neither of these imperfections is expected to be of practical relevance for the receiver tracking and the overall signal quality appears well compatible with modernized signals of other GNSSs.

The CDMA constellation points are not visible themselves in the IQ diagram, but are described by the centers of four circles originating from the superimposed FDMA signals. Due to the lower frequency of the FDMA carrier, the chip transitions of the C/A- and P-code signals in the IQ plane rotate at a 2.37 MHz frequency in the CDMA-aligned IQ diagram and are smeared into circles around the CDMA

constellation points. The radius of this circle describes the combined IQ amplitude of the FDMA signal components, which is roughly 1.5 times lower than the corresponding CDMA amplitude. This confirms the earlier finding of a 3 dB higher total power of the CDMA signal compared to its FDMA counterpart.

Despite the high signal-to-noise ratio of IQ samples collected with the high-gain dish antenna, individual chip sequences of the CDMA signal cannot be easily distinguished in an I/Q-timeline plot due to the superposition of the FDMA signal, but require a priori knowledge of the individual ranging codes. Relevant specifications for the open service signal components are provided in the L1OC Interface Control Document (RSS 2016a). The ranging codes used for the L1OC data channel are Gold sequences (Gold 1967) with a length of 1023 chips obtained from 10-bit shift registers, while the ranging codes of the pilot channel are Kasami sequences (Kasami 1966) of length 4092 generated from 6- and 12-bit shift registers (RSS 2016a). Both codes are clocked at 0.5115 MHz resulting in a chip length of about 2 μs and repeat rates of 2 ms and 8 ms, respectively.

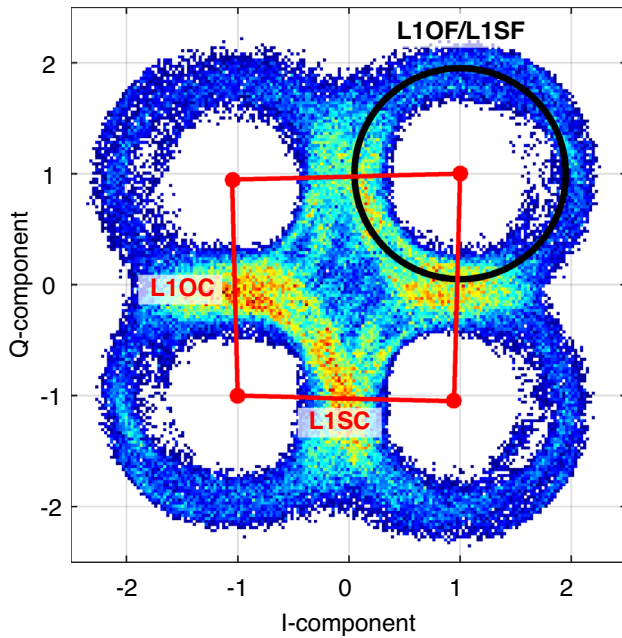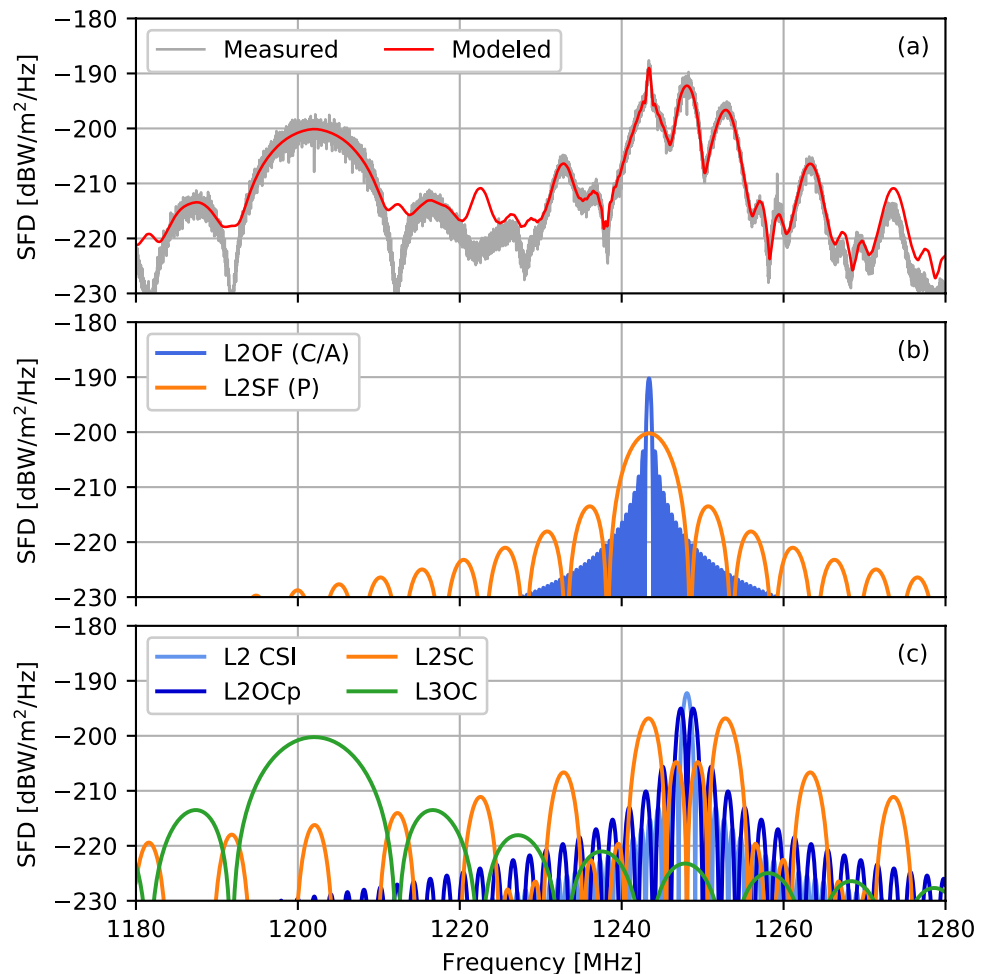**Fig. 3** CDMA-aligned IQ constellation diagram of the GLONASS-K2 L1 signal

Fig. 4 GLONASS-K2 (R803) spectrum in the L2+L3 frequency band as collected with the Weilheim 30-m dish-antenna on January 17, 2024 (**a**). For illustration, modeled infinite-bandwidth spectra of the individual FDMA signals (centered at 1243.375 MHz) and CDMA signals (L3 centered at 1202.025 MHz and L2 centered at 1248.06 MHz) signals are shown in panels (**b**) and (**c**), respectively. The sum of all these individual signals gives the *modeled* curve shown in red in panel (**a**)

The two codes are combined using a time multiplexing, in which the first half of the data channel chip is followed by the second half of the pilot chip. As such, individual code chips have an effective length of about 1 μs and give rise to BPSK(1) and BOC(1,1) spectra with characteristic lobes of 1 MHz width.

L2 and L3 signal components

In view of a virtually identical signal structure, the GLO-NASS-K2 spectrum in the L2 band closely resembles that of the L1 band. Main differences result from a slightly larger shift between the center frequencies of the CDMA signals centered at 1248.06 MHz and the FDMA signals centered at 1243.375 MHz for $k = -6$. As such, the peak of the L2 C/A-code signal in Fig. 4 collected during the initial testing in early 2024 coincides roughly with the left main lobe of the BOC(5,2.5)-modulated L2SC signal.

The observed spectral flux density of the L2 signals at the time of data collection is roughly 3 dB smaller than that of the L1 signal, but otherwise shows a very similar power sharing among the individual components. It should be

noted, though, that the ratio of the L1/L2 flux depends on the respective gains of the transmit antenna in viewing direction and does not necessarily reflect the total transmit power ratio for the two frequencies. Other than for GPS, Galileo, and QZSS, no factory calibrations of the GLONASS antennas have been released so far that would allow a concise mapping of the measured EIRP to the actual transmit power (Steigenberger et al. 2018).

The IQ constellation diagram of the L2 signal obtained after removal of the Doppler-shifted CDMA carrier frequency is shown in Fig. 5. It closely resembles the corresponding L1 results and exhibits similar deviations from the nominal phase alignment of the I and Q components. However, a slightly lower amplitude of the FDMA signal relative to the CDMA may be recognized. It indicates a roughly 4 dB CDMA/FDMA power difference in good accord with signal power estimates derived from the spectrum in Fig. 4.

At its lower end, the L2 spectrum of the K2 satellite overlaps with that of the L3OC signal. The latter signal is transmitted with a center frequency of 1202.025 MHz and shows the characteristic spectrum of a BPSK(10) modulation. It is actually made up of two components with equal amplitude that are combined in phase quadrature (RSS 2016c). The combined power of the in-phase (I) an quadrature (Q) channels roughly equals that of the L2SC signal and the L2 P-code power by roughly 3 dB. The received flux of the combined I and Q components corresponds to an EIRP of 28.5 dBW, which is about 1 dB lower than that of the L2OS and L2OC(CSI+pilot) signal.
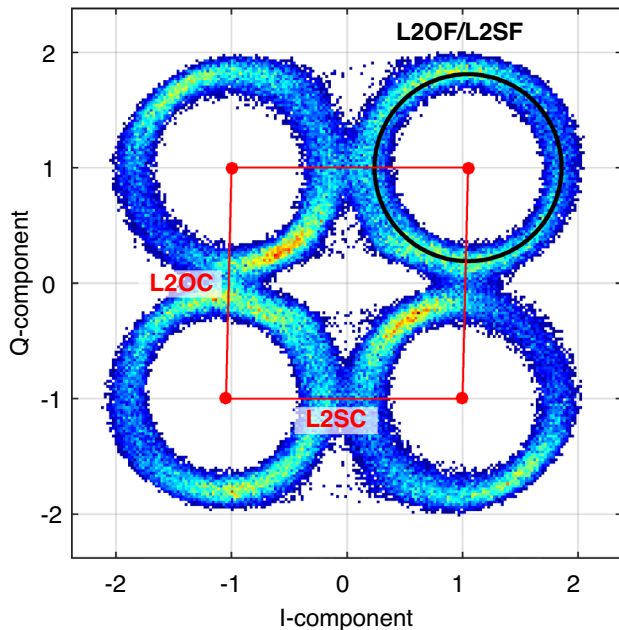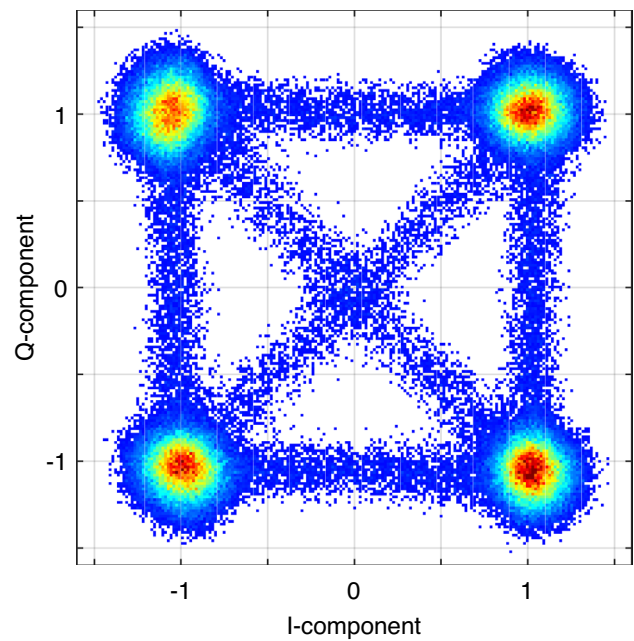

Fig. 6 IQ constellation plot of the GLONASS-K2 L3 signal

The IQ constellation diagram of the L3OC signal is shown in Fig. 6. It shows an almost ideal square geometry reflecting a QPSK modulation with equal amplitude in the I- and Q-component. Similar to the very first transmissions on the GLONASS-K1 satellite (Thoelert et al. 2011), its clean chip transitions hint at a largely digital signal generation. Only a very minor distortion of the IQ states may be recognized which can originate from band limitations or saturation of the navigation signal generator and amplifier.

The ranging codes of the L2OC pilot component are Kasami sequences obtained from 7- and 14-bit shift registers with a length of 10230 chips (RSS 2016b). The code generator matches that of the L3OC signal and uses identical initial values for the respective shift registers, but the signal is transmitted with a different chipping rate (see Tab. 1). While the L3OC ranging code is cycled at 10 MHz and has a duration of 1 ms, the L2OCp code uses a 0.5115 MHz rate and is repeated once every 20 ms. The L2 CSI ranging code is presently unpublished but has been identified to employ a Gold code matching that of the L1OCd signal. It is time-multiplexed with the L2OCp channel in the same way as the data and pilot components of the L1OC signal. The identification of the CSI range code generator enabled collection of independent observations for the two L2OC channels with a prototype receiver as discussed in the next section.

Fig. 5 CDMA-aligned IQ constellation plot of the GLONASS-K2 L2 signal

Receiver tracking

Initial short-period or single-frequency transmission of L1 and L2 FDMA signals of R803 started on 8 September 2023 with the slot number R26 and frequency channel number $k = -6$. Continuous transmission of L1/L2 FDMA as well as the L3 CDMA signal started on 11 September 2023 around 14:00. In December 2023, R803 switched for a 7-day period to slot number R25 and frequency channel number $k = -5$, see Table 2. In January 2024, another week with a different frequency channel number ($k = -7$) occurred but with the same slot number.

Table 2 GLONASS R803 signal transmission with different slot and frequency channel numbers

Start	End	Slot	Freq. Ch.
08 Sep 2023	07 Dec 2023	R26	−6
08 Dec 2023	14 Dec 2023	R25	−5
14 Dec 2023	05 Jan 2024	R26	−6
05 Jan 2024	12 Jan 2024	R26	−7
12 Jan 2024		R26	−6

As of March 2024, R26 L1 and L2 FDMA signals are tracked by a reasonable amount of modern GNSS receivers of the IGS station network. The L3 signal is only tracked by a subset of these receivers due to configuration or firmware issues. The L1 and L2 CDMA signals are currently tracked by none of the IGS stations. A prototype firmware supporting GLONASS CDMA tracking on all three frequencies was installed on two JAVAD TRE_3S GNSS receivers operated by DLR/GSOC. The GSOC04DEU station located in Oberpfaffenhofen, Germany, is configured to separately track data and pilot signals while UNX400AUS in Sydney, Australia, performs a combined tracking of data and pilot components of the CDMA signals. Both receivers are connected to a Leica AR25.R3 antenna with LEIT radome. Figure 7 shows the carrier-to-noise density ratio (C/N_0) of different generations of GLONASS satellites tracked by these two receivers. Data of an 8-day time interval, i.e., the GLONASS ground track repeat period, in January/February 2024 were averaged per individual receiver.

GLONASS-M satellites transmit the L1 and L2 FDMA signals with lower transmit power than the newer generations of GLONASS satellites (Steigenberger et al. 2018). P- and C/A-code signals in Fig. 7a differ by up to 1 dBHz and the L1 signals show a 5–8 dBHz higher C/N_0 compared
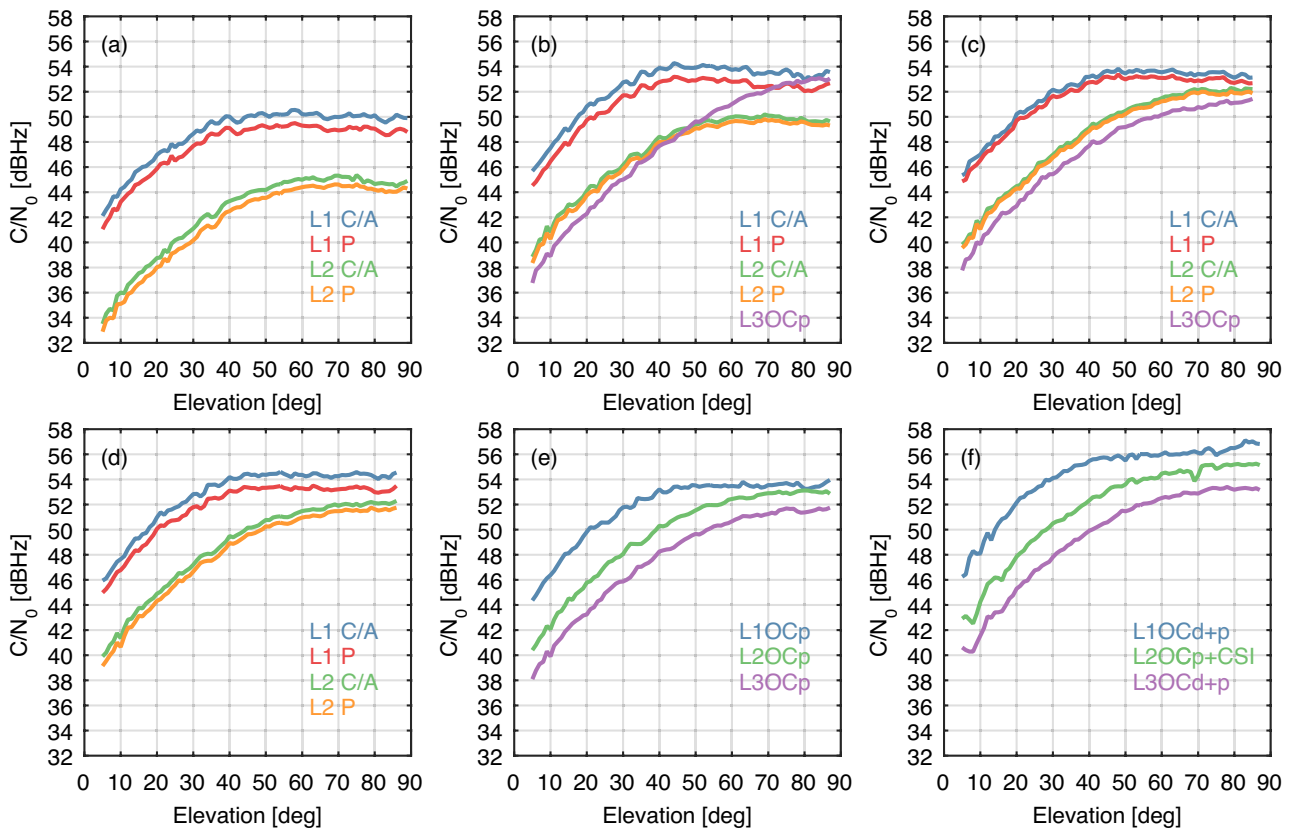

Fig. 7 Carrier-to-noise density ratio of different types of GLONASS satellites and signals. **a** GLONASS-M (R730); **b** GLONASS-M+ (R860); **c** GLONASS-K1B (R806); **d–f** GLONASS-K2 (R803). Panels **a–e** are based on data of GSOC04DEU, panel **f** is based on data of UNX400AUS

to L2. GLONASS-M+ (Fig. 7b) shows higher C/N$_0$ values for both, the L1 and L2 FDMA signals with peak values of 54 dBHz for L1 C/A and 50 dBHz for L2 C/A. The C/N$_0$ pattern of the L3OCp signal follows the L2 signal for elevations up to 45°. For higher elevations the L3OCp C/N$_0$ further increases up to a maximum of 54 dBHz. This behavior is related to the separate L3 transmit antenna, which is composed of a single helix element only resulting in a higher gain at low boresight angles.

For GLONASS-K1B shown in Fig. 7c, all signals are transmitted by the same antenna. Thus, the L3OCp C/N$_0$ pattern closely follows the L2 pattern but with a 1 dBHz lower magnitude. Whereas the L1 pattern of M+ and K1B are very similar, the L2 CDMA signals of K1B have up to 2 dBHz higher C/N$_0$ values for elevations above 50°. This behavior might be explained by an updated design of the K1B transmit antenna.

GLONASS-K2 FDMA signals in Fig. 7d essentially show the same behavior as those of GLONASS-K1B in Fig. 7c indicating that the same antenna design is used for the FDMA antenna of K2 and the K1B antenna. C/N$_0$ measurements for the pilot components of the CDMA signals are shown in Fig. 7e. The observed L1OCp C/N$_0$ is roughly 1 dBHz lower compared to L1 C/A. L2 C/A and L2OCp have similar C/N$_0$ values for very low elevations but L2OCp outperforms L2 C/A by up to 1 dBHz for higher elevations. The results are essentially consistent with the relative transmit powers of individual components discussed in the previous section, when allowing for uncertainties at the 1 dB level in the employed C/N$_0$ estimators (Petovello 2010).

The time-multiplexed data and pilot components of the L1, L2 and L3 CDMA signals are modulated with a 1:1 power ratio (RSS 2016a, b, c). Thus, a 3 dBHz higher C/N$_0$ is expected for the combined tracking of both signal components compared to data- or pilot-only tracking. This is roughly confirmed by the measured increase of about 2 dBHz shown in Fig. 7f.

The pseudorange noise and multipath characteristics of the R803 tracking at the GSOC04DEU site are illustrated in Fig. 8. The graph shows the root-mean square magnitude of noise and multipath errors as a function of elevation as obtained from the dual-frequency multipath combinations (Rocken and Meertens 1992; Kee and Parkinson 1994)

$$\text{MP}_i = P_i - \phi_i - \frac{2 \cdot f_j}{f_i^2 - f_j^2} \cdot \left(\phi_i - \phi_j \right) \qquad (2)$$

of pseudorange and carrier phase observations P and ϕ at frequencies f_i and f_j.

The L1 and L2 FDMA open service signals L1 C/A and L2 C/A show the largest RMS with mean values of 101 and 93 cm, respectively. For elevations up to 35°, they are almost identical whereas L2 C/A outperforms L1 C/A by
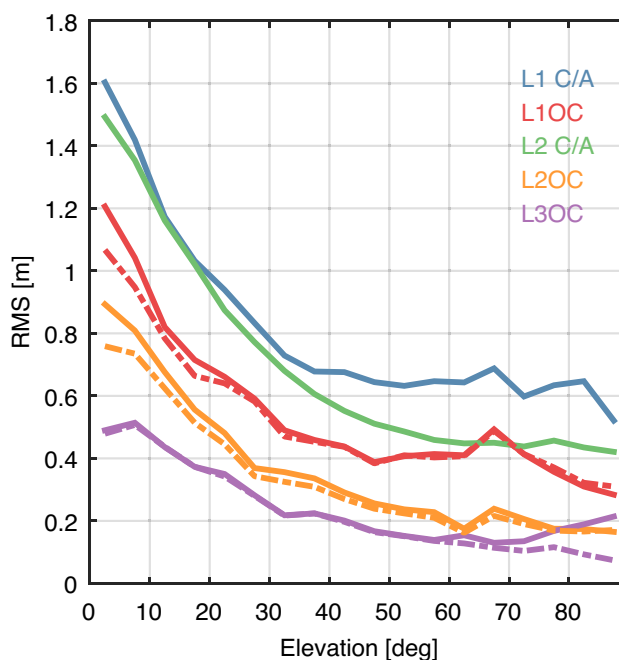

Fig. 8 GLONASS R803 noise and multipath of the station GSOC-04DEU in Oberpfaffenhofen, Germany. For the CDMA signals, the solid lines refer to the data/CSI component, the dash-dotted lines to the pilot component

up to 20 cm for higher elevations. The L1 CDMA tracking results in 25–52% smaller RMS values compared to L1 C/A. Data and pilot tracking provide almost identical performance and only show a marginal benefit of the BOC modulation on the pilot channel over the BPSK-modulated data channel resulting in mean RMS values of 71 and 67 cm, respectively. The L2 CDMA noise/multipath obtained with the present receiver is smaller by 18–60% compared to L1 CDMA. The mean RMS values are 53 cm for L2 CSI and 48 cm for L2OCp. The L3OC signals shows the best multipath/noise characteristics due to its large bandwidth of 10 MHz giving a mean RMS value of 33 cm and differences between data and pilot tracking only for elevations above 60°.

The coherency of different signals can be evaluated by a geometry- and ionosphere-free linear combination of carrier phase observations at three frequencies. The dual-frequency ionosphere-free linear combination

$$\text{IF}_{i,j} = \frac{f_i}{f_i^2 - f_j^2} \cdot \phi_i - \frac{f_j}{f_i^2 - f_j^2} \cdot \phi_j. \qquad (3)$$

eliminates the first order ionospheric effect. The difference $\text{GFIF}_{i,j,k} = \text{IF}_{i,j} - \text{IF}_{i,k}$ of two IF linear combinations formed from three different frequencies furthermore eliminates the geometric contributions including range, clock offsets and tropospheric delays. It is nominally constant except for contributions like carrier phase measurement noise, multipath,
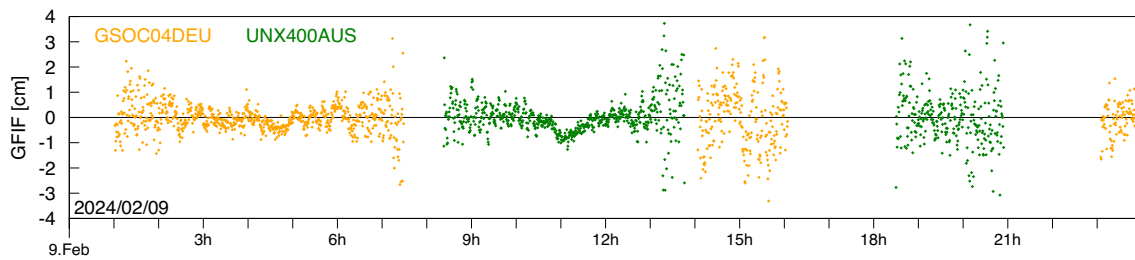
Fig. 9 GLONASS R803 geometry- and ionosphere-free linear combination obtained from L1/L2/L3 CDMA carrier phase observations of the stations GSOC04DEU at Oberpfaffenhofen, Germany, and UNX400AUS at Sydney, Australia

inter-frequency phase biases, and ambiguities of the individual signals (Simsky 2006). Montenbruck et al. (2012) found orbit-periodic GFIF variations for the GPS Block IIF satellites. Their amplitude depends on the elevation of the Sun above the orbital plane and can reach values up to 20 cm.

Figure 9 shows the GLONASS R803 GFIF linear combination for L1/L2 and L1/L3 CDMA signals of the Sydney and Oberpfaffenhofen stations on February 9, 2024. The GFIF essentially shows increased noise at low elevations as well as multipath-induced variations for the second half of the first pass at GSOC04DEU. No orbit-periodic variations are visible confirming the consistency of the three carriers among each other. However, a 1 cm dip can be seen in the GFIF of UNX400AUS at around 11:00. This dip occurs for elevations about 70° corresponding to a boresight angle of 6.5°. It is also visible for GSOC04DEU as well as for other days if that elevation is exceeded and can potentially be explained by elevation- and frequency-dependent phase patterns of the transmit antenna.

Summary and conclusions

The activation of the first GLONASS-K2 satellite in September 2023 represents a major milestone in the history of the the Russian Global'naya Navigatsionnaya Sputnikova Sistema, GLONASS. It finally marks the transition from frequency division multiple access (FDMA) signals to code division multiple access (CDMA) signals across all frequency bands. We provide a first analysis of the new L1 and L2 CDMA signals using a high-gain 30-m dish antenna and independent measurements with a prototype receiver supporting both FDMA and CDMA tracking. The combination of BPSK(1), BOC(1,1), and BOC(5,2) modulations offers a clean separation of open service and secured service components in the new signal. The high-gain antenna spectra suggest the absence of bandpass limitations and clearly show the signal sidelobes over a range of more than ± 50 MHz relative to the respective center frequencies. The combined signal power in the two open service channels of the L1 and L2 CDMA signals is roughly two times (3 dB) higher than that of the FDMA C/A-code signals. CDMA IQ constellation diagrams are affected by the superposition of FDMA signals transmitted by a separate antenna in adjacent frequencies, but indicate clean chip transitions representative of a digital signal generation unit. For the data channel of the open L2 CDMA signal, which is reserved for the "channel for service information" (CSI) and currently lacks a public specification, use of a Gold code similar to the L1OCd channel is identified based on analysis of the high-gain antenna data.

The ranging measurements collected with a prototype receiver confirm the increased CDMA signal power as well as the improved noise and multipath characteristics of the new modulations. Even though differential code biases (DCBs) cannot presently be assessed with just a single satellite transmitting the new L1 and L2 CDMA signals, a notably reduced scatter of satellite DCBs across the future GLONASS constellation can be expected compared to the current FDMA signals. Furthermore, ambiguity resolution in precise point positioning (PPP) applications will be greatly facilitated by the use of common signal frequencies for all satellites. Even though several launches of new GLONASS satellites are planned for the upcoming years, it remains unclear, so far, by what time a sufficient number of satellites will transmit L1 and L2 signals for an initial CDMA navigation service.

Author Contributions ST collected and analyzed the high-gain antenna measurements. PS performed the GNSS receiver data analysis. All authors contributed to the discussion and interpretation of results and critically reviewed the final manuscript.

Declarations

Conflict of interest The authors have no conflict of interest that are relevant to the content of this article.

References

Bakitko R (2021) Comparative analysis of methods of formation of navigation radiosignals of GLONASS system and features of group navigation radio signals. Rocket Space Device Eng Inf Syst 8(2):62–71. https://doi.org/10.30894/issn2409-0239.2021.8.2.62.71

Biryukov AA (2018) Variant of technical realization of non-linear multiplexing GLONASS FDMA and CDMA navigation signals. Rocket Space Device Eng Inf Syst 5(2):10–17

Gold R (1967) Optimal binary sequences for spread spectrum multiplexing. IEEE T Inf Theory 13(4):619–621. https://doi.org/10.1109/TIT.1967.1054048

Johnston G, Riddell A, Hausler G (2017) The International GNSS Service. In: Teunissen P, Montenbruck O (eds) Springer Handbook of Global Navigation Satellite Systems, Springer, chap 33, pp 967–982. https://doi.org/10.1007/978-3-319-42928-1_33

Karutin S (2012) GLONASS signals and augmentations. Proc ION GNSS 2012:3878–3911

Karutin S (2023) GLONASS: the decade of transition to CDMA signals. GPS World 34(12):39–41

Kasami T (1966) Weight distribution formula for some class of cyclic codes, R-285. University of Illinois Urbana-Champaign, Champaign

Kee C, Parkinson B (1994) Calibration of multipath errors on GPS pseudorange measurements. Proc ION GPS 1994:353–362

Langley RB (1997) GLONASS: review and update. GPS World 8(7):46–51

Lennen GR (1989) The USSR's Glonass P-code-determination and initial results. Proc ION GPS 1989:77–83

Maqsood M, Gao S, Montenbruck O (2017) Antennas. In: Teunissen P, Montenbruck O (eds) Springer Handbook of Global Navigation Satellite Systems, Springer, chap 17, pp 505–534. https://doi.org/10.1007/978-3-319-42928-1_17

Montenbruck O, Günther C, Graf S, Garcia-Fernandez M, Furthner J, Kuhlen H (2006) GIOVE-A initial signal analysis. GPS Solut 10(2):146–153. https://doi.org/10.1007/s10291-006-0027-7

Montenbruck O, Hugentobler U, Dach R, Steigenberger P, Hauschild A (2012) Apparent clock variations of the Block IIF-1 (SVN62) GPS satellite. GPS Solut 16(3):303–313. https://doi.org/10.1007/s10291-011-0232-x

Petovello M (2010) Carrier-to-noise algorithms. InsideGNSS 5(1):20–26

PNT IAC (2020) Global navigation satellite system GLONASS open service performance standard (OS PS), edition 2.2; Information and Analysis Center for Positioning, Navigation and Timing (PNT IAC). Central Research Institute of Machine Building, Korolev

Revnivykh S, Bolkunov A, Serdyukov A, Montenbruck O (2017) GLONASS. In: Teunissen P, Montenbruck O (eds) Springer Handbook of Global Navigation Satellite Systems. Springer, chap 8, pp 219–245. https://doi.org/10.1007/978-3-319-42928-1_8

RISDE (2008) GLONASS interface control document: Navigation radiosignals in bands L1, L2; version 5.1; Russian Institute of Space Device Engineering

Rocken C, Meertens C (1992) UNAVCO receiver tests, memo 8. UNAVCO, Boulder

RSS (2016a) GLONASS interface control document: Code division multiple access open service navigation signal in L1 frequency band, edition 1.0; Russian Space Systems, JSC

RSS (2016b) GLONASS interface control document: Code division multiple access open service navigation signal in L2 frequency band, edition 1.0; Russian Space Systems, JSC

RSS (2016c) GLONASS interface control document: Code division multiple access open service navigation signal in L3 frequency band, edition 1.0; Russian Space Systems, JSC

Simsky A (2006) Three's the charm. Triple-frequency combinations in future GNSS. InsideGNSS 1(4):38–41

Steigenberger P, Thoelert S, Montenbruck O (2018) GNSS satellite transmit power and its impact on orbit determination. J Geod 92(6):609–624. https://doi.org/10.1007/s00190-017-1082-2

Thoelert S, Erker S, Meurer M (2009) GNSS signal verification with a high gain antenna—calibration strategies and high quality signal assessment. Proc ION ITM 2009. Portland, Oregon, pp 289–300

Thoelert S, Erker S, Furthner J, Meurer M, Gao G, Heng L, Walter T, Enge P (2011) First signal in space analysis of GLONASS K-1. Proc ION GNSS 2011:3076–3082

Thoelert S, Meurer M, Erker S, Montenbruck O, Hauschild A, Fenton P (2012) A multi-technique approach for characterizing the SVN49 signal anomaly, part 2: chip shape analysis. GPS Solut 16(1):29–39. https://doi.org/10.1007/s10291-011-0204-1

Thoelert S, Antreich F, Enneking C, Meurer M (2019) BeiDou 3 signal quality analysis and its impact on users. Navigation 66(4):695–704. https://doi.org/10.1002/navi.331

Thoelert S, Steigenberger P, Montenbruck O, Meurer M (2019) Signal analysis of the first GPS III satellite. GPS Solut 23(4):92. https://doi.org/10.1007/s10291-019-0882-7

Zaminpardaz S, Teunissen PJ, Nadarajah N (2017) GLONASS CDMA L3 ambiguity resolution and positioning. GPS Solut 21(2):535–549. https://doi.org/10.1007/s10291-016-0544-y

Publisher's Note Springer Nature remains neutral with regard to jurisdictional claims in published maps and institutional affiliations.

Steffen Thoelert received his diploma degree in electrical engineering from the University of Magdeburg in 2002. In May 2006, he joined the Institute of Communications and Navigation at DLR Oberpfaffenhofen. His current research activities include signal quality monitoring, satellite payload characterization, GNSS threat detection and modeling.

Peter Steigenberger received his master and PhD degrees in Geodesy from Technische Universität München (TUM) in 2002 and 2009, respectively. Currently, he is a senior researcher at DLR's German Space Operations Center (GSOC). His research interests focus on GNSS data analysis, in particular precise orbit and clock determination of GNSS satellites and the evolving navigation systems Galileo, BeiDou, and QZSS.

Oliver Montenbruck is head of the GNSS Technology and Navigation Group at DLR's German Space Operations Center, where he started work as a flight dynamics analyst in 1987. His current research activities comprise space-borne GNSS receiver technology, autonomous navigation systems, spacecraft formation flying, precise orbit determination, and multi-constellation GNSS.